Supporting Information

Bimetallic and Postsynthetic Alloyed PtCu Nanostructures with Tunable Reactivity toward Methanol Oxidation Reaction

Haiyan Xiang,[†,a] Yueshao Zheng,[‡,a] Yue Sun,[†] Tingting Guo,[§] Pei Zhang,[†] Wei Li,[†] Shiwei Kong,[†] Miray Ouzounian,[∥] Hong Chen,[⊥] Huimin Li,[†] Travis Shihao Hu,[∥,*] Gang Yu,[†,*] Yexin Feng,[‡,*] and Song Liu[†,*]

[†] Institute of Chemical Biology and Nanomedicine (ICBN), State Key Laboratory of Chemo/Biosensing and Chemometrics, College of Chemistry and Chemical Engineering, Hunan University, Changsha 410082, P. R. China

[‡] Hunan Provincial Key Laboratory of Low-Dimensional Structural Physics and Devices, School of Physics and Electronics, Hunan University, Changsha 410082, P. R. China

[§] Key Laboratory of Yunnan Provincial Higher Education Institutions for Organic Optoelectronic Materials and Devices, Kunming University, Kunming 650000, P. R. China

[∥] Department of Mechanical Engineering, California State University, Los Angeles, CA 90032, USA

[⊥] School of Materials Science and Energy Engineering, Foshan University, Foshan 528000, P. R. China

*Corresponding authors:
E-mail: liusong@hnu.edu.cn (S. Liu)
Email: yexinfeng@hnu.edu.cn (Y. X. Feng)
E-mail: yuganghnu@163.com (G. Yu)
E-mail: shu17@calstatela.edu (T. S. Hu)

[a] H. Y. Xiang and Y. S. Zheng contributed equally to this work

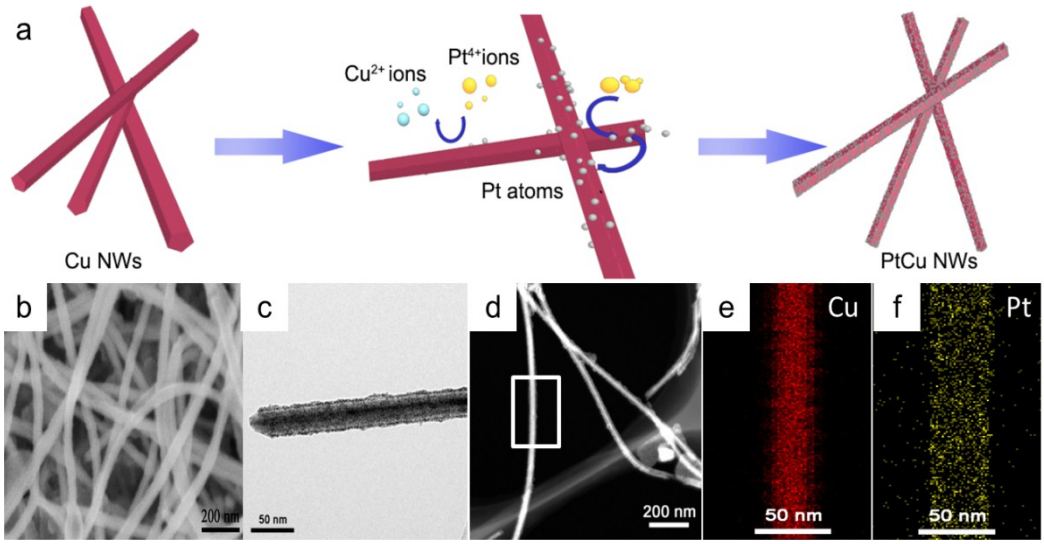

Fig S1. (a) Schematic illustration the PtCu nanowires formation (with 5 mL H_2PtCl_4) process without ascorbic acid. (b) SEM image, (c) TEM image, (d) HAADF-STEM image and corresponding element mapping (Cu and Pt) (e, f) of PtCu nanowires without ascorbic acid.

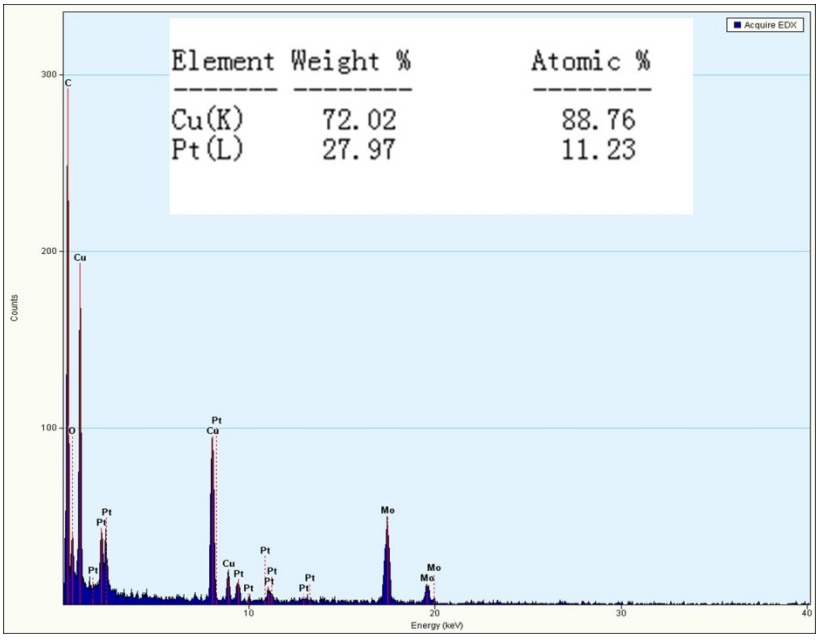

Fig S2. EDS pattern of PtCu nanowires without ascorbic acid. (with 5 mL H_2PtCl_4).

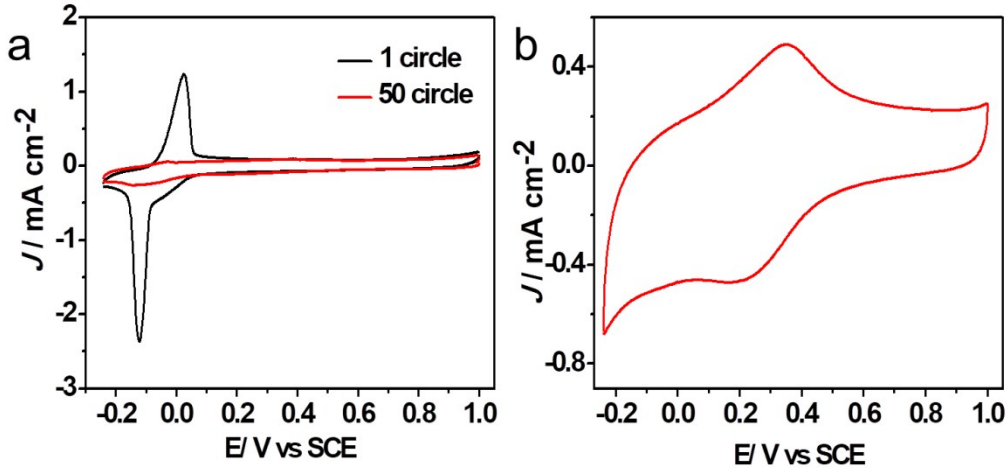

Fig S3. (a) CV curves of PtCu nanowires without ascorbic acid in 0.1 M $HClO_4$ solution, and in (b) 0.1 M $HClO_4$ + 0.5M CH_3OH solution at a scan rate of 50 $mV \cdot s^{-1}$

Table S1. Precursor solutions with different AA, H_2PtCl_4, and PVP·K30

Constitute	$Pt_{14}Cu_{86}$	$Pt_{59}Cu_{41}$	$Pt_{67}Cu_{33}$	$Pt_{78}Cu_{22}$	$Pt_{81}Cu_{19}$	$Pt_{90}Cu_{10}$
AA (mL)	2.4	6	12	25	30	36
H_2PtCl_4 (mL)	2	5	10	20	25	30
PVP·K30 (g)	0.2	0.5	1	2	2.5	3

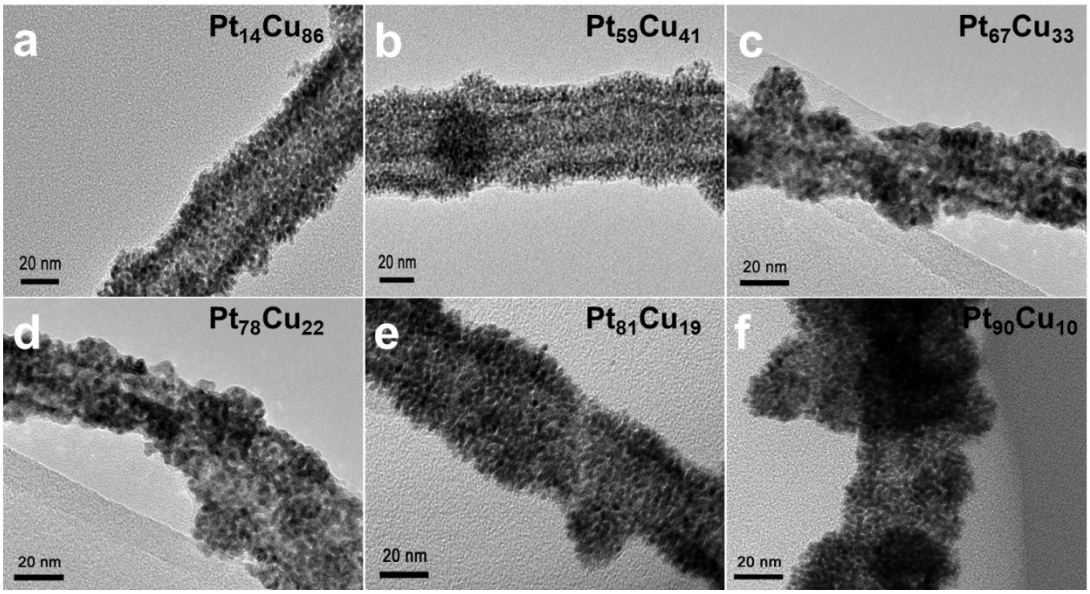

Fig S4. TEM images of (a) $Pt_{14}Cu_{86}$, (b) $Pt_{59}Cu_{41}$, (c) $Pt_{67}Cu_{33}$, (d) $Pt_{78}Cu_{22}$, (e) $Pt_{81}Cu_{19}$ and (f) $Pt_{90}Cu_{10}$ with ascorbic acid.

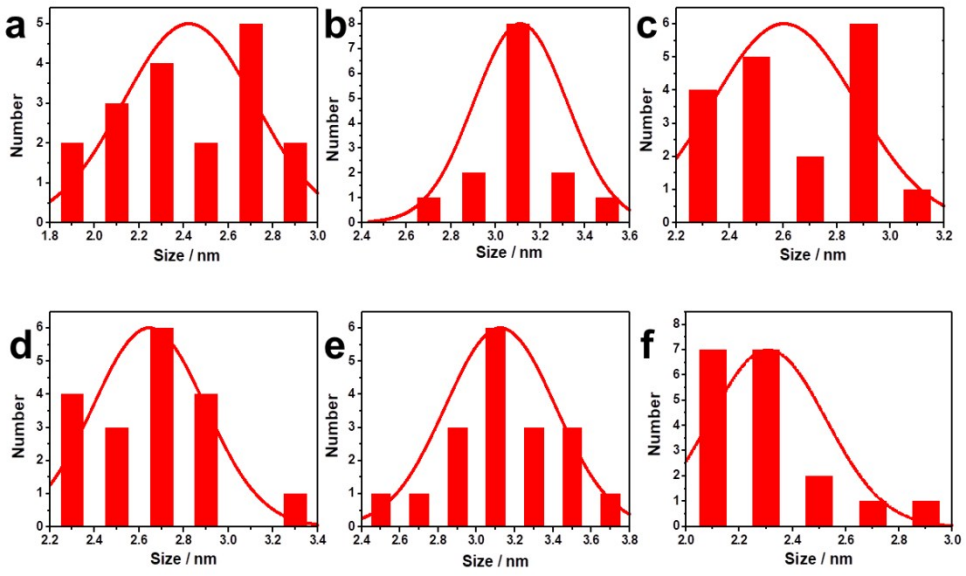

Fig S5. Pt nanoparticles diameter distribution of (a) $Pt_{14}Cu_{86}$, (b) $Pt_{59}Cu_{41}$, (c) $Pt_{67}Cu_{33}$, (d) $Pt_{78}Cu_{22}$, (e) $Pt_{81}Cu_{19}$ and (f) $Pt_{90}Cu_{10}$ with ascorbic acid from Fig S4 corresponding TEM images.

Table S2. Composition of XRD, TEM data of PtCu without annealed process

Constitute	$2\theta_{111}$	d_{111} (nm)	FWHM	LP (nm)	D_{crys} (nm)	TEM (nm)
$Pt_{14}Cu_{86}$	40.664	0.2217	3.924	0.3841	2.03	2.42
$Pt_{59}Cu_{41}$	40.292	0.2236	2.219	0.3873	3.815	3.09
$Pt_{67}Cu_{33}$	40.106	0.2246	2.243	0.3890	3.772	2.60
$Pt_{78}Cu_{22}$	40.097	0.2247	2.159	0.3891	3.919	2.64
$Pt_{81}Cu_{19}$	40.060	0.2249	2.197	0.3895	3.850	2.30
$Pt_{90}Cu_{10}$	40.057	0.2249	2.426	0.3895	3.490	3.11

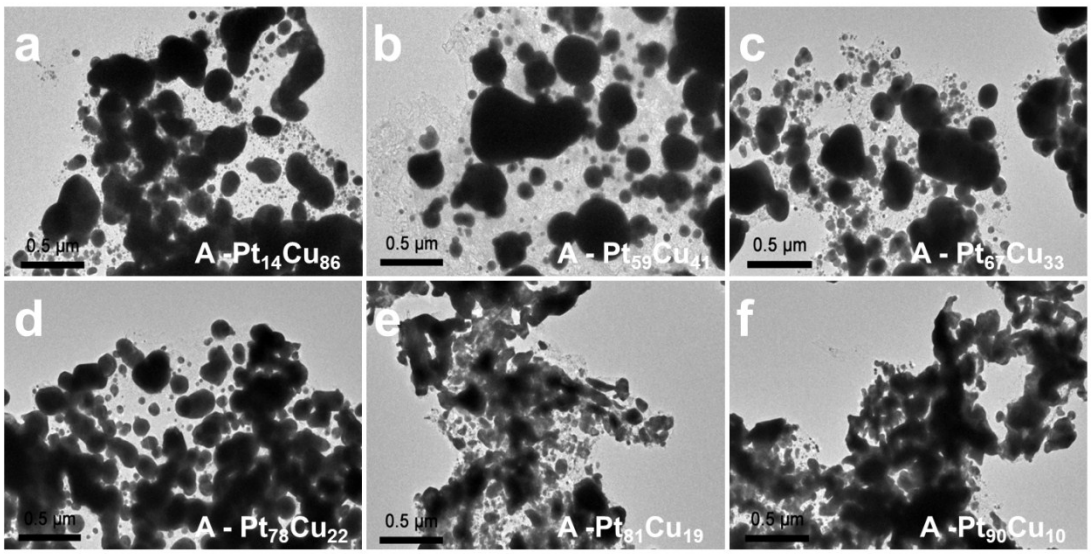

Fig S6. TEM images of (a) A-$Pt_{14}Cu_{86}$, (b) A-$Pt_{59}Cu_{41}$, (c) A-$Pt_{67}Cu_{33}$, (d) A-$Pt_{78}Cu_{22}$, (e) A-$Pt_{81}Cu_{19}$ and (f) A-$Pt_{90}Cu_{10}$ after 800 °C annealed.

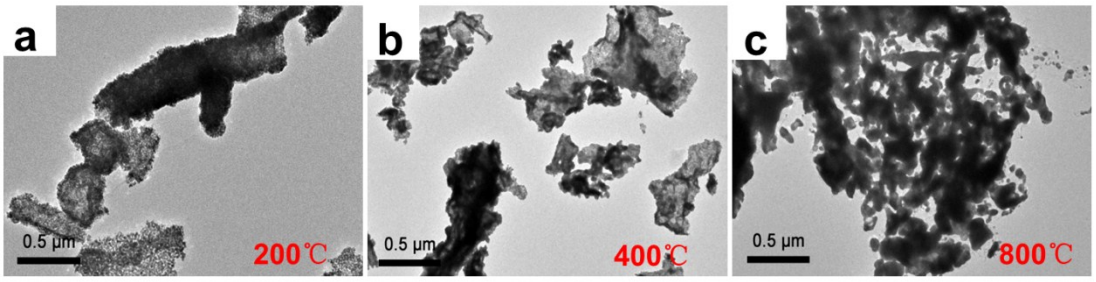

Fig S7. SEM images of A-$Pt_{90}Cu_{10}$ after 200 (a), 400 (b) and 800 °C (c) annealed.

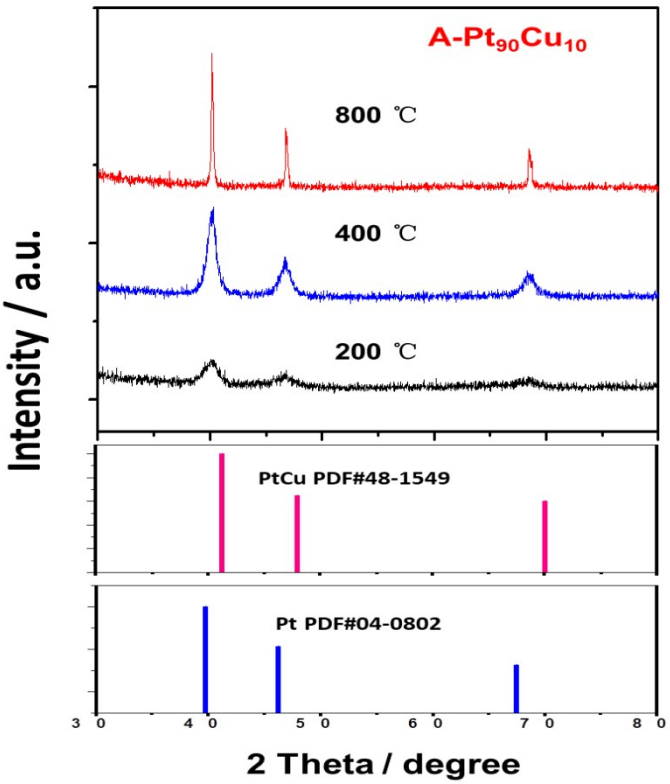

Fig S8. XRD patterns of A-$Pt_{90}Cu_{10}$ after 200, 400 and 800 °C annealed.

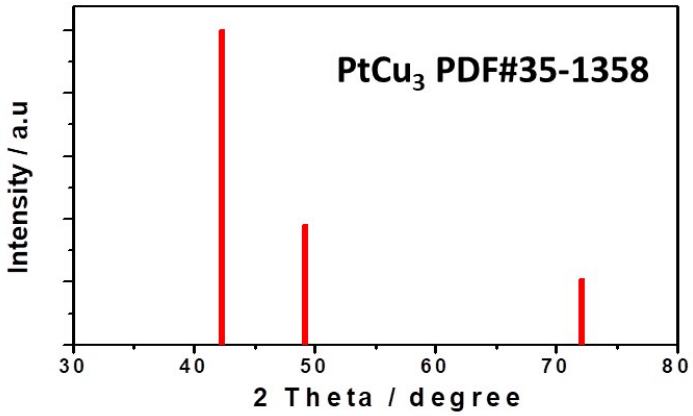

Fig S9. XRD pattern of standard PDF $PtCu_3$ (JCPDS No. 35−1358).

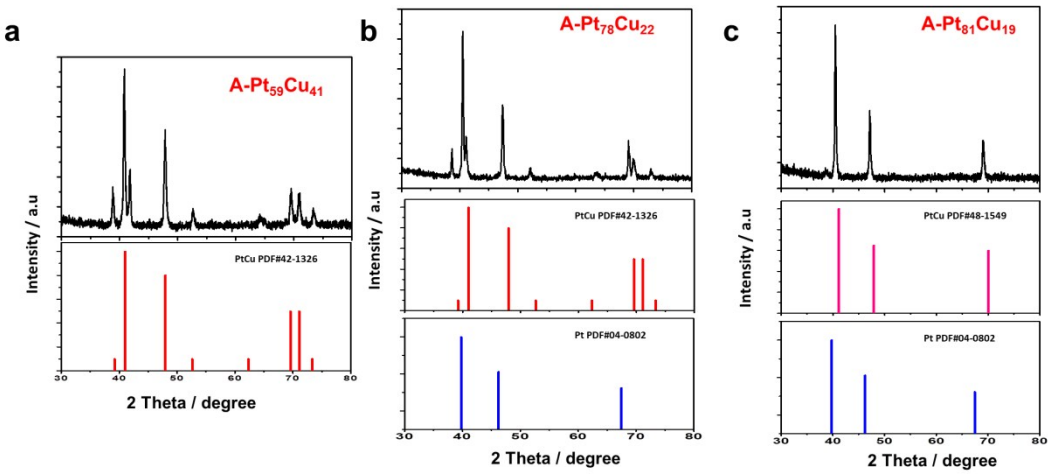

Fig S10. XRD patterns of (a) A-$Pt_{59}Cu_{41}$, and (b) A-$Pt_{78}Cu_{22}$ and (c) A-$Pt_{81}Cu_{19}$ after 800 °C annealed.

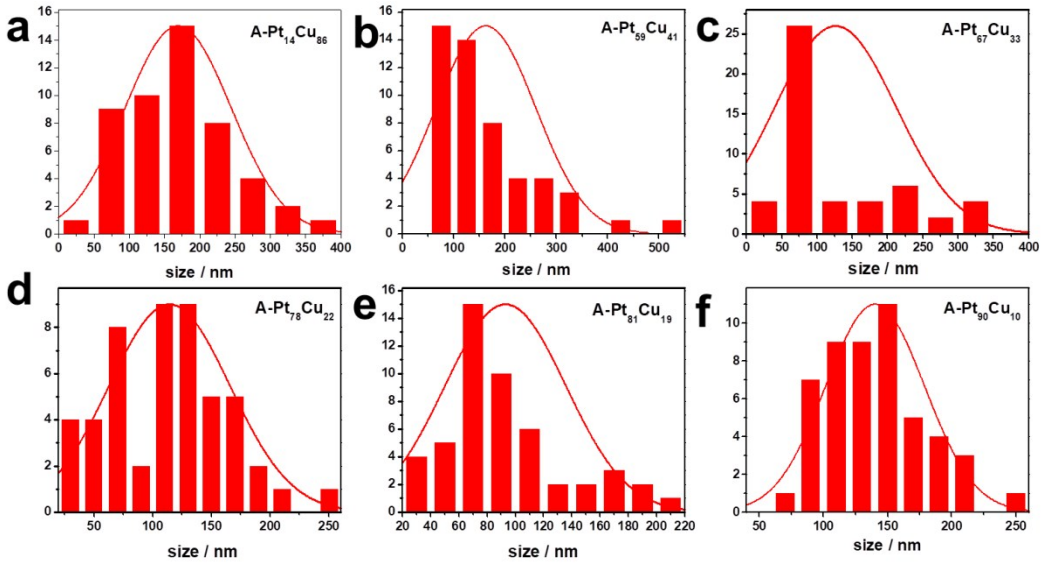

Fig S11. PtCu nanoparticles diameter distribution of (a) A-$Pt_{14}Cu_{86}$, (b) A-$Pt_{59}Cu_{41}$, (c) A-$Pt_{67}Cu_{33}$, (d) A-$Pt_{78}Cu_{22}$, (e) A-$Pt_{81}Cu_{19}$ and (f) A-$Pt_{90}Cu_{10}$ after 800 °C annealed from Fig S6 corresponding TEM images.

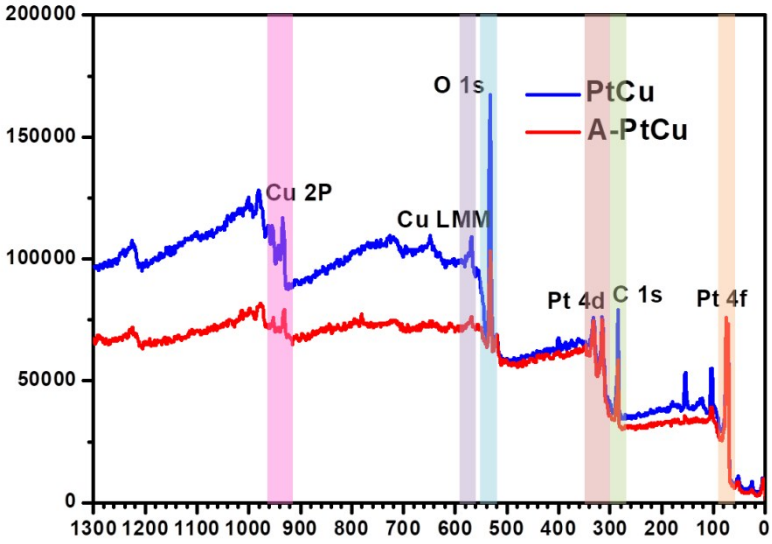

Fig S12. XPS spectra of $Pt_{67}Cu_{33}$ and after 800 °C annealed PtCu.

Table S3. Composition of XRD, TEM data of PtCu annealed at 800 ℃

Constitute	$2\theta_{111}$	d_{111} (nm)	FWHM	LP (nm)	D_{crys} (nm)	TEM (nm)
A-$Pt_{14}Cu_{86}$	42.212	0.2139	0.287	0.3705	27.922	168.78
A-$Pt_{59}Cu_{41}$	40.814	0.2209	0.334	0.3826	23.950	162.80
A-$Pt_{67}Cu_{33}$	40.726	0.2217	0.225	0.3834	35.550	128.06
A-$Pt_{78}Cu_{22}$	40.540	0.2220	0.270	0.3851	29.620	114.00
A-$Pt_{81}Cu_{19}$	40.478	0.2227	0.293	0.3856	27.300	94.14
A-$Pt_{90}Cu_{10}$	40.230	0.2243	0.240	0.3879	33.330	139.20

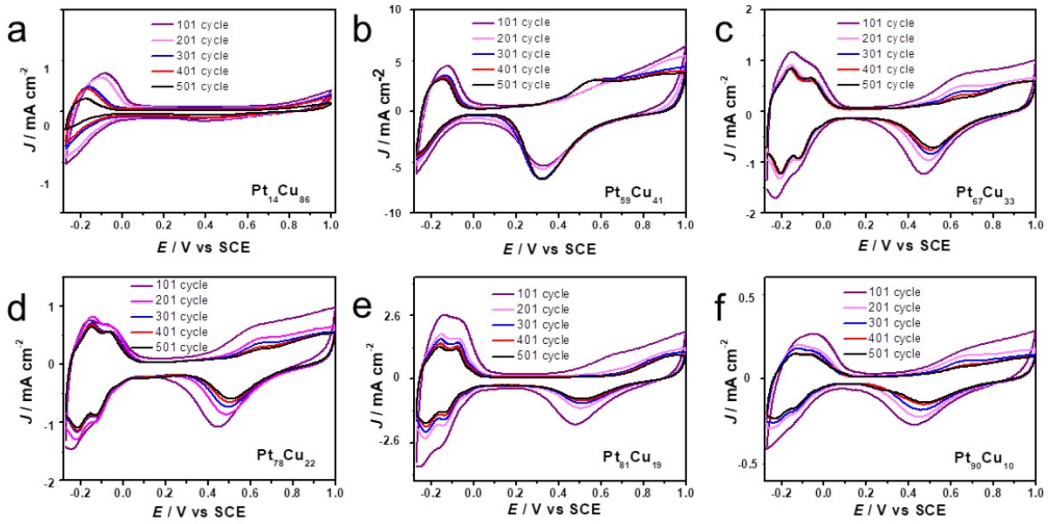

Fig S13. CV 500 circles curves of (a) $Pt_{14}Cu_{86}$, (b) $Pt_{59}Cu_{41}$, (c) $Pt_{67}Cu_{33}$, (d) $Pt_{78}Cu_{22}$, (e) $Pt_{81}Cu_{19}$ and (f) $Pt_{90}Cu_{10}$ before annealed products in 0.1 M $HClO_4$ solution.

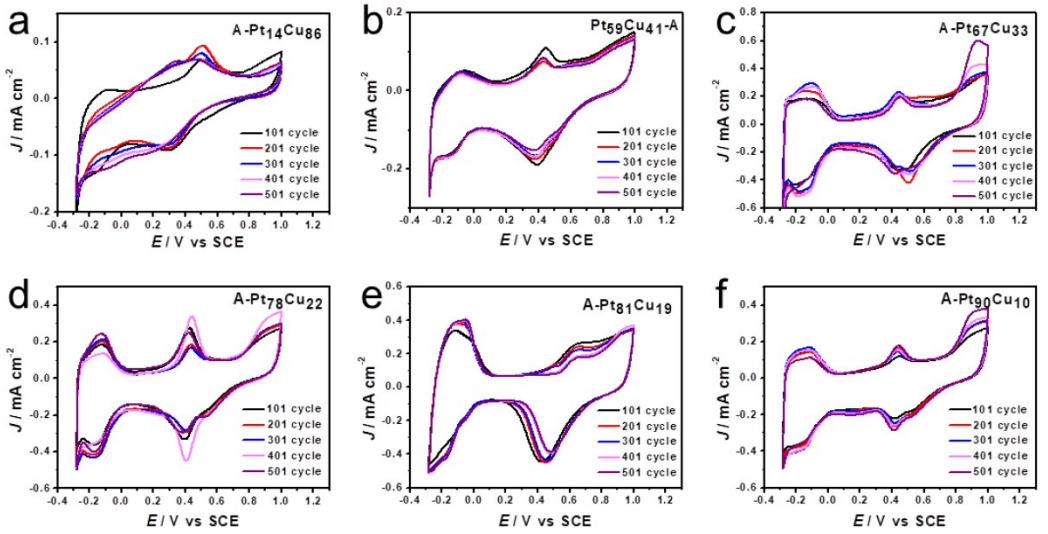

Fig S14. CV 500 circles curves of (a) A-$Pt_{14}Cu_{86}$, (b) A-$Pt_{59}Cu_{41}$, (c) A-$Pt_{67}Cu_{33}$, (d) A-$Pt_{78}Cu_{22}$, (e) A-$Pt_{81}Cu_{19}$ and (f) A-$Pt_{90}Cu_{10}$ after 800 °C annealed in 0.1 M $HClO_4$ solution.

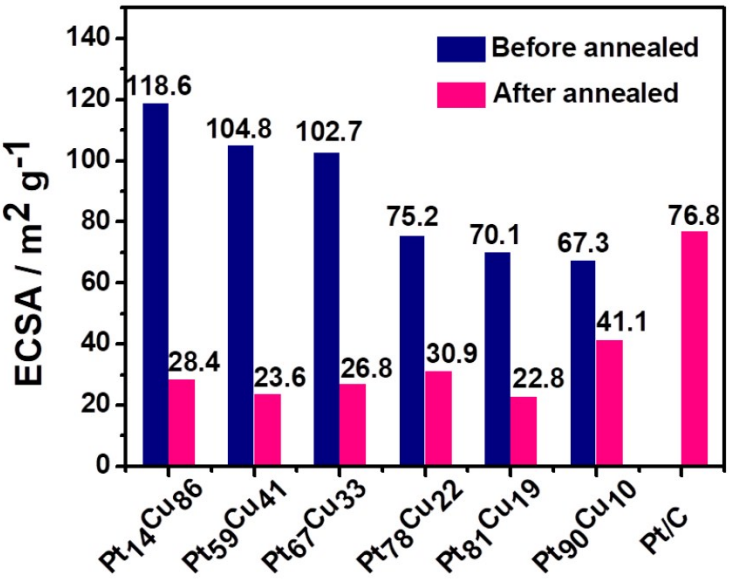

Fig S15. ECSA histogram of (a) $Pt_{14}Cu_{86}$, (b) $Pt_{59}Cu_{41}$, (c) $Pt_{67}Cu_{33}$, (d) $Pt_{78}Cu_{22}$, (e) $Pt_{81}Cu_{19}$ and (f) $Pt_{90}Cu_{10}$ before and after annealed in 0.1 M $HClO_4$ solution.

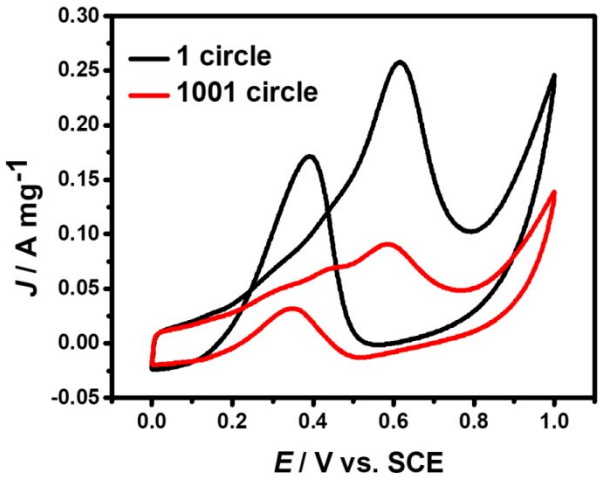

Fig S16. CV curves durability of Pt/C in 0.1 M $HClO_4$+0.5 M CH_3OH solution at 0.55 V.

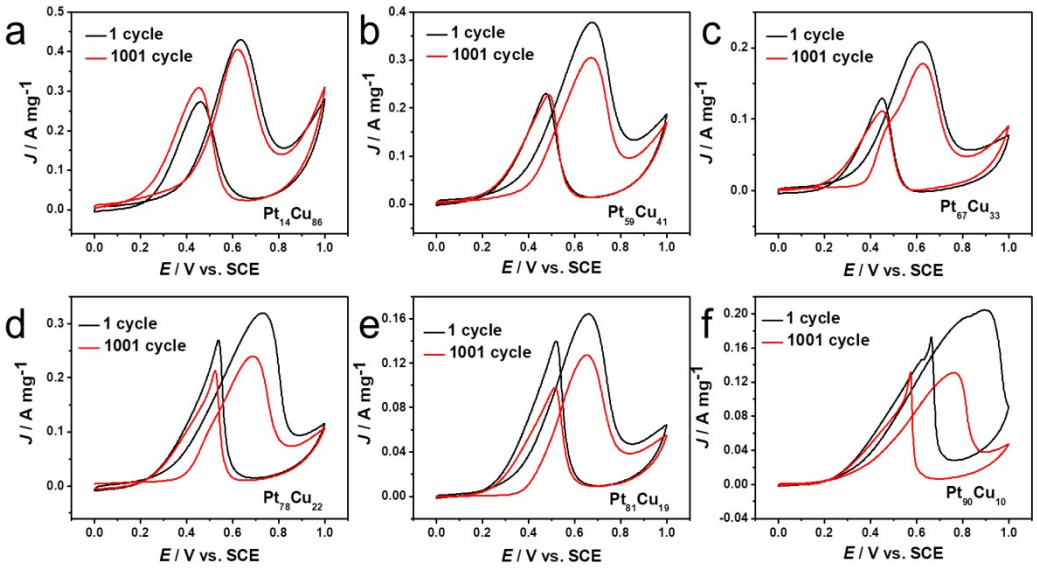

Fig S17. CV curves durability of (a) $Pt_{14}Cu_{86}$, (b) $Pt_{59}Cu_{41}$, (c) $Pt_{67}Cu_{33}$, (d) $Pt_{78}Cu_{22}$, (e) $Pt_{81}Cu_{19}$ and (f) $Pt_{90}Cu_{10}$ before annealed products in 0.1 M $HClO_4$+0.5 M CH_3OH solution at 0.55 V.

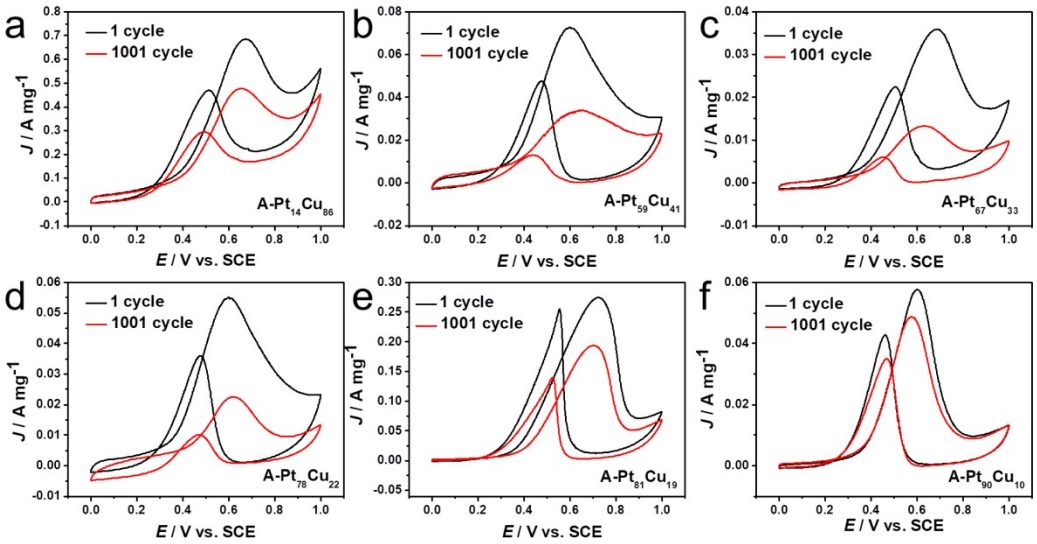

Fig S18. CV curves durability of (a) A-$Pt_{14}Cu_{86}$, (b) A-$Pt_{59}Cu_{41}$, (c) A-$Pt_{67}Cu_{33}$, (d) A-$Pt_{78}Cu_{22}$, (e) A-$Pt_{81}Cu_{19}$ and (f) A-$Pt_{90}Cu_{10}$ after 800 °C annealed in 0.1 M $HClO_4$+0.5 M CH_3OH solution at 0.55 V.

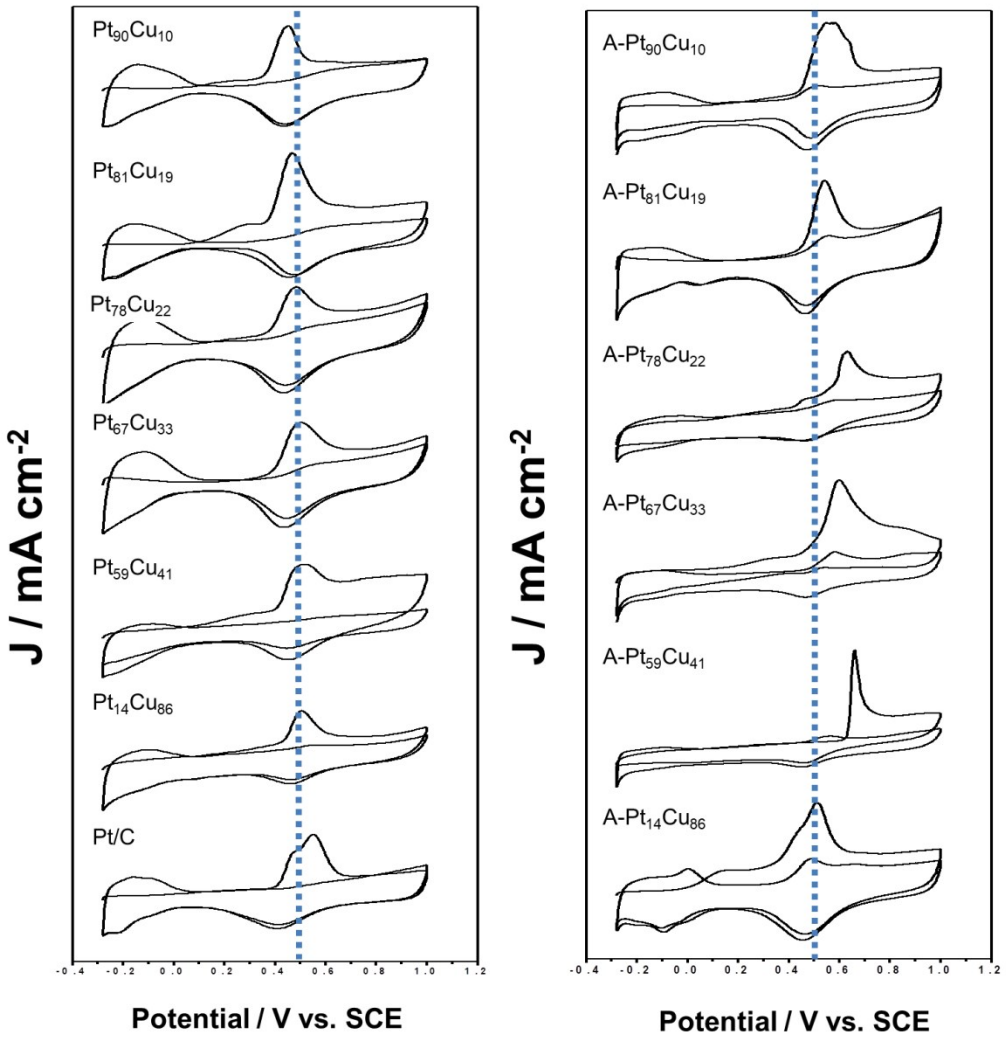

Fig S19. CO stripping curves of (a) $Pt_{14}Cu_{86}$, (b) $Pt_{59}Cu_{41}$, (c) $Pt_{67}Cu_{33}$, (d) $Pt_{78}Cu_{22}$, (e) $Pt_{81}Cu_{19}$ and (f) $Pt_{90}Cu_{10}$ before (left) and after (right) annealed in 0.1 M $HClO_4$ solution at a scan rate of 50 mV s^{-1}.

Table S4. CO stripping potential of different composition catalysis

Constitute	$Pt_{14}Cu_{86}$	$Pt_{59}Cu_{41}$	$Pt_{67}Cu_{33}$	$Pt_{78}Cu_{22}$	$Pt_{81}Cu_{19}$	$Pt_{90}Cu_{10}$	Pt/C
Before annealed (V)	0.502	0.515	0.504	0.507	0.468	0.451	0.548
After annealed (V)	0.511	0.663	0.605	0.631	0.541	0.544	0.548

Table S5. Electrochemical properties of different composition PtCu before annealed

Constitute	$Pt_{14}Cu_{86}$	$Pt_{59}Cu_{41}$	$Pt_{67}Cu_{33}$	$Pt_{78}Cu_{22}$	$Pt_{81}Cu_{19}$	$Pt_{90}Cu_{10}$	Pt/C
ECSA (m^2 g^{-1})	118.6	104.8	102.7	75.2	70.1	67.3	76.8
SA (mA cm^{-2})	0.7069	0.8899	0.7790	1.319	1.1314	2.113	1.09
MA (mA mg^{-1})	429.6	378.6	208.21	319.8	164.4	204.4	257.0
			After 1000 cycles				
MA (A mg^{-1})	405.0	305.3	177.8	239.9	127.1	130.8	91.0

Table S6. Electrochemical properties of different composition A-PtCu after annealed at 800 ℃

Constitute	$Pt_{14}Cu_{86}$	$Pt_{59}Cu_{41}$	$Pt_{67}Cu_{33}$	$Pt_{78}Cu_{22}$	$Pt_{81}Cu_{19}$	$Pt_{90}Cu_{10}$	Pt/C
ECSA (m^2 g^{-1})	28.40	23.55	25.34	30.89	22.88	41.14	76.8
SA (mA cm^{-2})	9.2607	1.73	1.34	1.74	7.07	2.91	1.09
MA (A mg^{-1})	685.5	72.8	22.4	54.9	274.5	57.7	257.0
			After 1000 cycles				
MA (A mg^{-1})	476.1	32.8	13.3	22.5	194.01	48.8	91.0

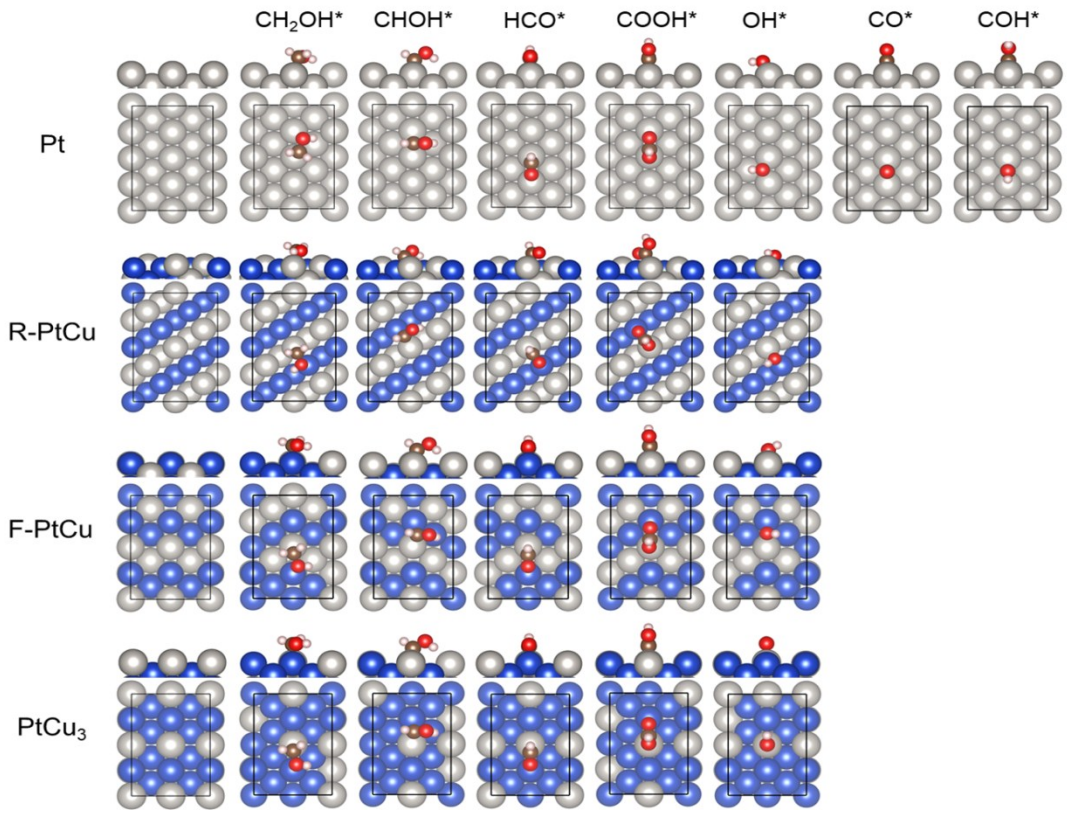

Fig S20. Top and side views of fully relaxed systems of clean Pt, R-PtCu, F-PtCu and $PtCu_3$ {110} surface as well as intermediates during methanol electrooxidation. Blue, gray, red, brown and white spheres correspond to Cu, Pt, O, C and H atoms, respectively.

Table S7 Elementary steps of three reaction paths for MOR. The * stands for different catalyst surfaces; CH_2OH*, CHOH*, HCO*, COH*, COOH*, CO* and OH* are absorbed intermediates.

	Path 1	Path 2	Path 3
S1	$CH_3OH+*\rightarrow CH_2OH*+H^++e^-$	$CH_3OH+*\rightarrow CH_2OH*+H^++e^-$	$CH_3OH+*\rightarrow CH_2OH*+H^++e^-$
S2	$CH_2OH+*\rightarrow CHOH*+H^++e^-$	$CH_2OH+*\rightarrow CHOH*+H^++e^-$	$CH_2OH+*\rightarrow CHOH*+H^++e^-$
S3	$CHOH+*\rightarrow HCO*+H^++e^-$	$CHOH+*\rightarrow HCO*+H^++e^-$	$CHOH+*\rightarrow COH*+H^++e^-$
S4	$HCO*+H_2O+*\rightarrow HCO*+OH*+H^++e^-$	$HCO*\rightarrow CO*+H^++e^-$	$COH*\rightarrow CO*+H^++e^-$
S5	$HCO*+OH*\rightarrow COOH*+H^++e^-+*$	$CO*+H2O+*\rightarrow CO*+OH*+H^++e^-$	$CO*+H2O+*\rightarrow CO*+OH*+H^++e^-$
S6	$COOH*\rightarrow CO_2+*+H^++e^-$	$CO*+OH*\rightarrow CO_2+*+*+H^++e^-$	$CO*+OH*\rightarrow CO_2+*+*+H^++e^-$

Table S8 The calculated Gibbs free energy (ΔG) of three reaction paths for MOR on Pt {110} surface.

Elementary	Path 1	Path 2	Path 3
steps	ΔG	ΔG	ΔG
(S1)	-0.575	-0.575	-0.575
(S2)	-0.375	-0.375	-0.375
(S3)	0.185	0.185	0.520
(S4)	0.215	-0.825	-1.160
(S5)	-0.015	0.215	0.215
(S6)	0.435	1.245	1.245

Table S9 The predicted Gibbs free energy (ΔG) of path 1 in methanol electrooxidation on Pt, R-PtCu, F-PtCu and $PtCu_3$ {110} surface.

Elementary	Pt	R-PtCu	F-PtCu	$PtCu_3$
steps	ΔG	ΔG	ΔG	ΔG
(S1)	-0.575	-0.155	-0.005	-0.255
(S2)	-0.375	0.105	0.125	0.075
(S3)	0.185	-0.165	-0.355	-0.305
(S4)	0.215	0.345	0.325	-0.045
(S5)	-0.015	-0.185	-0.225	0.155
(S6)	0.435	-0.075	0.005	0.245